Magnetic properties of f-electron systems in spin-polarized relativistic density functional theory

1997 J. Phys.: Condens. Matter 9 10881

(http://iopscience.iop.org/0953-8984/9/49/008)

J. Phys.: Condens. Matter **9** (1997) 10881–10900. Printed in the UK PII: S0953-8984(97)86467-3

Magnetic properties of f-electron systems in spin-polarized relativistic density functional theory

H Yamagami†, A Mavromaras and J Kübler

Institut für Festkörperphysik, Technische Hochschule, D-64289, Darmstadt, Germany

Received 31 July 1997, in final form 16 October 1997

Abstract. The magnetic ground state of the series of lanthanide and actinide trivalent ions is investigated by means of spin-polarized relativistic spin-density functional theory. In the local density functional approximation (LDA) an internal effective magnetic field due to exchange and correlation couples to the spin degrees of freedom. The resulting set of coupled Dirac equations yields ground-state multiplets that obey the well-known Hund's rules. This remarkable result comes about by the coupling of the $j = l + 1/2$ with the $j = l - 1/2$ states due to the exchange–correlation potential that is, as usual, the functional derivative of the exchange–correlation energy with respect to the spin magnetic moment. The effect of the coupling is shown to depend on the varying relative strengths of spin–orbit coupling and exchange splitting within the f series. Since in the f levels the *internal* exchange splitting dominates rather than the spin–orbit splitting, the energy level scheme is that of the Paschen–Back effect, and thus features of the Russell–Saunders coupling persist in spite of relativistic effects.

1. Introduction

Ab initio calculations based on spin-polarized density functional (SPDF) theory [1, 2] have become a standard tool in the investigation of electronic and magnetic properties of atoms, molecules and solids including open-shell systems [3]. In the series of the lanthanide and actinide elements the f electrons and the inner-core electrons are subject to a strong potential exerted by the nuclei [4]. Therefore a relativistic generalization of the density functional scheme with respect to the kinetic energy operator and the exchange–correlation energy was suggested by many authors [5–10] and the spin-polarized theory was completed by MacDonald and Vosko [6] and by Ramana and Rajagopal [8]. In this spin-polarized relativistic density functional (SPRDF) theory the Kohn–Sham equation consists of the one-electron Dirac equation containing an effective scalar potential and an additional effective magnetic field that is the functional derivative of the exchange–correlation energy with respect to the spin magnetic moment only. This is an approximation in which orbital contributions to the magnetic moment are neglected [11]. Since a complete methodology is currently unavailable this so-called spin-only Dirac theory is believed to be a reasonable starting point for the description of electronic and magnetic properties of f-electron systems.

In the series of 4f and 5f atoms and ions the occupation of the f shell, or alternatively the outer d shell, increases with the atomic number while the occupation of the outer s and p shells remains unchanged [12]. Furthermore the distribution of the f electrons is confined to the space inside the outer shells; thus, if these atoms are brought together to form

† Permanent address: Graduate School of Science, Physics Department, Tohoku University, Sendai 980-77, Japan.

0953-8984/97/4910881+20$19.50

molecules or solids, the f electrons do not directly participate in the chemical bonding. As a consequence the magnetic properties of f-electron metals are largely given by those of the corresponding free ions. It is in this spirit that we attempt to investigate the characteristics of f-electron systems by means of the SPRDF applied to the series of lanthanide and actinide ions.

In a central-field geometry the Kohn–Sham equation reduces to a radial equation that here becomes what we call the spin-polarized coupled Dirac (SPCD) equation. This was first solved in the framework of the Korringa–Kohn–Rostoker (KKR) multiple-scattering method [13–17] and a first self-consistent band-structure calculation of metallic Pu was performed using the linear muffin-tin orbital (LMTO) method [18]. Although self-consistent SPRDF calculations on ions, atoms and atomic cores in solids were also carried out [19, 20], a great deal of effort was put into the investigation of particular properties of a few isolated cases, while little attention was devoted to global trends such as energy splitting, wave functions, spin and orbital magnetic moments and Hund's rules for the formation of ground-state multiplets [21].

It is well known that Hund's rules describe in a nearly perfect manner the experimental findings for the ground states of the lanthanide ions. On the assumption that spin–orbit coupling has a rather small impact on moment formation in the 4f shell, the *Russell–Saunders* or *L–S* coupling scheme takes the spin and orbital angular moments to remain good quantum numbers. Hund's first and second rule, describing the order of filling of spin and orbital states for a given number of electrons, were explained by means of Hartree–Fock multiplet energy differences by Slater [22, 23]. Although the validity of the *L–S* coupling scheme seems to imply that the spin–orbit coupling has a negligible effect in the lanthanides, the 4f electrons are indeed subject to relativistic effects. As is clearly stated by Hund's third rule, it is the effect of spin–orbit coupling which completely lifts the remaining degeneracy of the 4f levels giving rise to distinct energy level splittings.

In this paper we describe self-consistent calculations of spin and orbital moments for trivalent ions belonging to the lanthanide and actinide series. These calculations are carried out with the SPCD equation employing the local density approximation (LDA) for the effective potential. The insertion of spin polarization into the Dirac equation leads to an infinite set of coupled equations. It was shown by Feder *et al* [13] and Strange *et al* [15] that the dominant terms are accounted for by an approximation where the coupling between $j = l + 1/2$ and $j = l - 1/2$ states is retained. We demonstrate that this coupling effect plays a key role in the formation of the ground-state moments as they are given by Hund's rules. Neglecting this coupling leads to the breakdown of Hund's rules. As will be seen from the energy splitting scheme later on, the physical situation in the f series, as it appears in the SPRDF, is subject to the interplay of the LDA exchange potential and the spin–orbit coupling. The SPCD equation provides the means to investigate the transition between the two limiting cases of strong exchange field on the one hand and dominating spin–orbit coupling on the other hand without any initial assumptions about the type of coupling characterizing a given ground-state multiplet.

The Dirac–Fock equations as they were outlined by [4] handle only pure *(jj)* coupled states. The Coulomb repulsion mixes different multiplets having the same total angular momentum, and therefore the ground state in Dirac–Fock theory has to be described by a linear combination of these configurations. In SPRDF theory it is the spin-split exchange potential that mixes initially independent single-particle states of different j into the ground-state wave function. It is this mixing as well as the release of any restrictions on the single-particle wave functions which open the way for the description of the intermediate-coupling scheme through linear combinations of orbitals of mixed j-character. Although we cannot

carry out any direct comparison with the Dirac–Fock method we stress the importance of the mixing of different js in the two approaches.

From the viewpoint of perturbation theory the energy levels of the f shell are generally dominated by the effects of *internal* exchange rather than those of spin–orbit coupling. In most cases considered, therefore, the nature of the energy splitting is more likely to be situated in the Paschen–Back regime [24]. This can be regarded as the reason for the Russell–Saunders coupling scheme holding despite the obvious influence of relativistic effects.

This paper is organized as follows. In section 2.1 the SPRDF theory is briefly outlined in the quantum electrodynamics formalism suggested by Rajagopal and Callaway [5] and the spin-only Dirac equation is derived. In section 2.2 this equation is shown to take the form of the SPCD equation in the case of a spherically symmetric potential as is typical for applications in ionic systems. A new algorithm for solving the resulting coupled first-order differential equation is described. Section 3 contains our results for lanthanide and actinide trivalent ions which include trends in the energy level splitting scheme as well as the shape of the radial wave functions and the spin and orbital magnetic moments that are discussed in the context of Russell–Saunders coupling. Finally section 4 contains our summary and conclusions.

2. The spin-polarized relativistic Hamiltonian

2.1. Spin-polarized relativistic density functional theory

In order to make this paper reasonably self-contained we briefly repeat the derivation of the one-electron spin-polarized relativistic equation for a system of interacting electrons in an external scalar potential $V_{ext}(\boldsymbol{r})$ and an external magnetic field $\boldsymbol{B}_{ext}(\boldsymbol{r})$ $(=\boldsymbol{\nabla}\times\boldsymbol{A}_{ext}(\boldsymbol{r}))$, as originally outlined by Rajagopal and Callaway [5]. In quantum electrodynamics (QED) the fully relativistic Hamiltonian, $\hat{H}$, is described in terms of the four-current operator $(\hat{n}(\boldsymbol{r}), \hat{\boldsymbol{J}}(\boldsymbol{r}))$. The energy of the ground state, $|\Psi\rangle$, is written using the field operator $\hat{\psi}(\boldsymbol{r})$ as

$$E = \langle\Psi|\hat{H}|\Psi\rangle = \langle\Psi|\hat{H}_0|\Psi\rangle + \int \mathrm{d}\boldsymbol{r}\left[V_{ext}(\boldsymbol{r})n(\boldsymbol{r}) - \frac{e}{c}\boldsymbol{A}_{ext}(\boldsymbol{r})\cdot\boldsymbol{J}(\boldsymbol{r})\right] \tag{2.1}$$

where e and c denote the electron charge and the velocity of light, respectively. The charge density $n(\boldsymbol{r})$ is given by

$$n(\boldsymbol{r}) = \langle\Psi|\hat{n}(\boldsymbol{r})|\Psi\rangle = \langle\Psi|\hat{\psi}^{\dagger}(\boldsymbol{r})\hat{\psi}(\boldsymbol{r})|\Psi\rangle \tag{2.2}$$

while the current density $\boldsymbol{J}(\boldsymbol{r})$ is

$$\boldsymbol{J}(\boldsymbol{r}) = \langle\Psi|\hat{\boldsymbol{J}}(\boldsymbol{r})|\Psi\rangle = \langle\Psi|\hat{\psi}^{\dagger}(\boldsymbol{r})c\beta\boldsymbol{\alpha}\hat{\psi}(\boldsymbol{r})|\Psi\rangle. \tag{2.3}$$

Here $\boldsymbol{\alpha}$ and β denote the standard Dirac 4×4 matrices [25] and $\hat{H}_0$ the relativistic Hamiltonian that is composed of the relativistic kinetic energy, the Coulomb interaction of the electronic system, the energy of a free radiation field as well as the interaction between the electron and the transverse radiation field.

The Hohenberg–Kohn theorems [26, 27] were generalized to this formalism and the following statements were shown by [5, 11] to remain valid: (i) all ground-state properties are unique functionals of the four-current density; (ii) the ground-state energy is minimized in the ground-state density; associated with a given external field.

The Gordon decomposition for the relativistic current [28] singles out the spin moment and the result is the following expression for the ground-state energy:

$$E = \langle\Psi|\hat{H}_0|\Psi\rangle + \int \mathrm{d}\boldsymbol{r}\left[V_{ext}(\boldsymbol{r})n(\boldsymbol{r}) + \boldsymbol{B}_{ext}(\boldsymbol{r})\boldsymbol{m}_s(\boldsymbol{r}) - \frac{e}{c}\boldsymbol{J}_{orb}(\boldsymbol{r})\cdot\boldsymbol{A}_{ext}(\boldsymbol{r})\right]. \tag{2.4}$$

Here the spin-magnetization density, $\boldsymbol{m}_s(\boldsymbol{r})$, is defined in units of μ_B as

$$\boldsymbol{m}_s(\boldsymbol{r}) = \langle\Psi|\hat{\psi}^\dagger(\boldsymbol{r})\beta\boldsymbol{\sigma}\hat{\psi}(\boldsymbol{r})|\Psi\rangle \tag{2.5}$$

where $\boldsymbol{\sigma}$ is the Pauli matrix. $\boldsymbol{J}_{orb}(\boldsymbol{r})$ denotes the orbital current that is given by

$$\boldsymbol{J}_{orb}(\boldsymbol{r}) = \frac{1}{2m}\langle\Psi|\hat{\psi}^\dagger(\boldsymbol{r})\beta\tilde{\boldsymbol{p}}\hat{\psi}(\boldsymbol{r}) + [\beta\tilde{\boldsymbol{p}}\hat{\psi}(\boldsymbol{r})]^\dagger\hat{\psi}(\boldsymbol{r})|\Psi\rangle \tag{2.6}$$

where m is the electron mass and $\tilde{\boldsymbol{p}}$ denotes $\tilde{\boldsymbol{p}} = -\mathrm{i}\hbar\boldsymbol{\nabla} - e\boldsymbol{A}(\boldsymbol{r})/c$. The quantity $\boldsymbol{A}(\boldsymbol{r})$ is the vector potential stemming from the external and transverse part of the radiation field. Since the ground state under consideration is stationary, the time derivative of the polarization belonging to the spin gives no contribution to the ground-state energy. It is therefore omitted in equation (2.4).

In density functional theory the expectation value of $\hat{H}_0$, $\langle\Psi|\hat{H}_0|\Psi\rangle$, is usually given by

$$\langle\Psi|\hat{H}_0|\Psi\rangle = \langle\Psi|\hat{H}_s|\Psi\rangle + \int \mathrm{d}\boldsymbol{r}\int \mathrm{d}\boldsymbol{r}'\ \frac{n(\boldsymbol{r})n(\boldsymbol{r}')}{|\boldsymbol{r}-\boldsymbol{r}'|} + E_{xc}[n(\boldsymbol{r}), \boldsymbol{m}_s(\boldsymbol{r})] \tag{2.7}$$

where $\hat{H}_s$ is the single-particle Dirac Hamiltonian

$$\hat{H}_s = \int \mathrm{d}\boldsymbol{r}\ \hat{\psi}^\dagger(\boldsymbol{r})(c\boldsymbol{\alpha}\cdot\boldsymbol{p} + (\beta - I)mc^2)\hat{\psi}(\boldsymbol{r}). \tag{2.8}$$

Here $\boldsymbol{p} = -\mathrm{i}\hbar\boldsymbol{\nabla}$ is the momentum operator and I denotes the 4×4 unit matrix. The second term on the right-hand side of equation (2.7) is the Hartree energy while the third one is the exchange–correlation energy. We would like to stress that in this formalism E_{xc} is assumed to be a functional of $n(\boldsymbol{r})$ and $\boldsymbol{m}_s(\boldsymbol{r})$ only.

Varying the energy in equation (2.4) with respect to the basis functions $\varphi_i(\boldsymbol{r})$ of the field operator $\hat{\psi}(\boldsymbol{r})$ under the constraint of particle conservation in the N-electron system

$$\int \mathrm{d}\boldsymbol{r}\ n(\boldsymbol{r}) = N \tag{2.9}$$

we obtain the one-electron Dirac equation as follows:

$$\left[c\boldsymbol{\alpha}\cdot\boldsymbol{p} + (\beta - I)mc^2 + V(\boldsymbol{r}) + \beta\boldsymbol{\sigma}\cdot\boldsymbol{B}(\boldsymbol{r}) - \frac{e}{4mc^2}\beta\tilde{\boldsymbol{p}}\cdot\boldsymbol{A}_{ext}(\boldsymbol{r}) - \varepsilon_i\right]\varphi_i(\boldsymbol{r}) = 0. \tag{2.10}$$

Here $V(\boldsymbol{r})$ is the scalar potential,

$$V(\boldsymbol{r}) = V_{ext}(\boldsymbol{r}) + \int \mathrm{d}\boldsymbol{r}'\ \frac{2n(\boldsymbol{r}')}{|\boldsymbol{r}-\boldsymbol{r}'|} + \frac{\delta E_{xc}[n(\boldsymbol{r}), \boldsymbol{m}_s(\boldsymbol{r})]}{\delta n(\boldsymbol{r})} \tag{2.11}$$

and the magnetic field $\boldsymbol{B}(\boldsymbol{r})$ is

$$\boldsymbol{B}(\boldsymbol{r}) = \boldsymbol{B}_{ext}(\boldsymbol{r}) + \frac{\delta E_{xc}[n(\boldsymbol{r}), \boldsymbol{m}_s]}{\delta \boldsymbol{m}_s(\boldsymbol{r})} = \boldsymbol{B}_{ext}(\boldsymbol{r}) + \boldsymbol{B}_{xc}(\boldsymbol{r}). \tag{2.12}$$

Neglecting the fifth term on the left-hand side of equation (2.10) gives the spin-only Dirac equation as suggested by MacDonald and Vosko [6]. If the external magnetic field vanishes, i.e. $\boldsymbol{B}_{ext}(\boldsymbol{r}) = \boldsymbol{A}_{ext}(\boldsymbol{r}) = 0$, equation (2.10) reduces to

$$\left[c\boldsymbol{\alpha}\cdot\boldsymbol{p} + (\beta - I)mc^2 + V(\boldsymbol{r}) + \beta\boldsymbol{\sigma}\cdot\boldsymbol{B}_{xc}(\boldsymbol{r}) - \varepsilon_i\right]\varphi_i(\boldsymbol{r}) = 0. \tag{2.13}$$

If E_{xc} is defined as a functional of $n(\boldsymbol{r})$ and $\boldsymbol{m}_s(\boldsymbol{r})$ only, the SPRDF ground state of a system possessing spontaneous magnetic order is described by the spin-only Dirac equation.

2.2. Solution for atoms and ions

In order to investigate the magnetic properties of atoms and ions one defines the spin-quantization axis to be parallel to the z-direction in equation (2.13). Since the external scalar potential in equation (2.11) will be the spherically symmetric central potential due to the nucleus, the wave functions can be described by radial and spin-angular functions. As a basis set to represent spin-angular space in equation (2.11) a spin-angular function χ_κ^μ [25] constructed from the one-electron Dirac equation without a magnetic field is used. The spin-dependent potential then gives rise to coupling between states of the same μ where μ denotes the z-component of the total angular momentum j.

If the coupling between states of different orbital angular momentum is neglected, the infinite set of coupled equations becomes finite. In detail only interactions between two states $j = \ell \pm \frac{1}{2}$ of the same ℓ or, in terms of κ, $\kappa = +\ell$ and $-\ell - 1$ [25] are considered. This approximation was justified by a number of authors [13–15, 19] who showed that the effect of the neglected terms is of the order of $1/c^2$. However, we would like to mention that an investigation of the higher-order coupling was undertaken by Jenkins and Strange [17], but is not considered in this work. Thus the equations to be solved become (in rydberg units, where $\hbar = 1$, $m = 1/2$, $e^2 = 2$, $c = 274.072$):

$$\left[\frac{\mathrm{d}}{\mathrm{d}r} + \frac{\kappa}{r}\right] g_\kappa^\alpha(r) - \left[1 + \frac{E^\alpha - V(r) + B(r)\sigma^\mu_{-\kappa,-\kappa}}{c^2}\right] c f_\kappa^\alpha(r) = 0 \tag{2.14a}$$

$$\left[\frac{\mathrm{d}}{\mathrm{d}r} - \frac{\kappa}{r}\right] c f_\kappa^\alpha(r) + [E^\alpha - V(r) - B(r)\sigma^\mu_{\kappa,\kappa}] g_\kappa^\alpha(r) - B(r)\sigma^\mu_{\kappa,-\kappa-1} g^\alpha_{-\kappa-1}(r) = 0 \tag{2.14b}$$

$$\left[\frac{\mathrm{d}}{\mathrm{d}r} - \frac{\kappa+1}{r}\right] g^\alpha_{-\kappa-1}(r) - \left[1 + \frac{E^\alpha - V(r) + B(r)\sigma^\mu_{\kappa+1,\kappa+1}}{c^2}\right] c f^\alpha_{-\kappa-1}(r) = 0 \tag{2.14c}$$

$$\left[\frac{\mathrm{d}}{\mathrm{d}r} + \frac{\kappa+1}{r}\right] c f^\alpha_{-\kappa-1}(r) + [E^\alpha - V(r) - B(r)\sigma^\mu_{\kappa,\kappa}] g^\alpha_{-\kappa-1}(r) - B(r)\sigma^\mu_{-\kappa-1,\kappa} g^\alpha_\kappa(r) = 0. \tag{2.14d}$$

Here $V(r)$ is the scalar potential as given by equation (2.11) and $B(r)$ is the z-component of the *internal* magnetic field due to exchange and correlation. The coefficients $\sigma^\mu_{\kappa,\kappa'}$ in equation (2.2) denote matrix elements of the Pauli spin matrix σ_z with the coupling states $\{\kappa\mu\}$ and $\{\kappa'\mu'\}$. They are given by the following equations:

$$\langle \chi_\kappa^\mu | \sigma_z | \chi_{\kappa'}^{\mu'} \rangle = \sigma^\mu_{\kappa,\kappa'} \delta_{\mu\mu'} = \begin{cases} -u_{\kappa\mu} & \text{for } \kappa' = \kappa \\ -\sqrt{1 - u^2_{\kappa\mu}} & \text{for } \kappa' = -\kappa - 1 \end{cases} \tag{2.15}$$

where $u_{\kappa\mu}$ is

$$u_{\kappa\mu} = \frac{\mu}{\kappa + 1/2}. \tag{2.16}$$

The two solutions of the above equation for a given $\{\ell\mu\}$ with their respective energies E^α are made up of a linear combination of *partial states* of κ and $-\kappa - 1$.

For $\mu = |\ell + 1/2|$ the last terms of equation (2.14*b*) and equation (2.14*d*) become zero because $\sigma^\mu_{\kappa,-\kappa-1} = \sigma^\mu_{-\kappa-1,\kappa} = 0$. Consequently the resulting solution will be of *pure* κ type for $\mu = |\ell + 1/2|$. The effect of the coupling is best appreciated if we compare with results from completely decoupled equations. Mainly for this purpose we omit the last two terms for all $\{\ell\mu\}$ and obtain two independent solutions with $\alpha = \kappa$ and $\alpha = -\kappa - 1$. In the following we refer to these as solutions of the *spin-polarized decoupled Dirac* (SPDD) equation which is also useful for obtaining starting electron densities.

In the coupled case (except for $\mu = |\ell + 1/2|$) the two different solutions labelled by α are characterized through their bonding and antibonding nature. In order to distinguish the two different types of solution for the same set of quantum numbers we suggest the use of the following parameters:

$$\eta_\alpha = \mathrm{sgn}\left[\int_0^\infty \mathrm{d}r\ (g_\kappa^\alpha(r) g_{-\kappa-1}^\alpha(r) + f_\kappa^\alpha(r) f_{-\kappa-1}^\alpha(r))\right] \tag{2.17}$$

and

$$\zeta_\alpha = \frac{1}{N}\int_0^\infty \mathrm{d}r\ (g_\kappa^\alpha(r)^2 + f_\kappa^\alpha(r)^2) \tag{2.18}$$

with the normalization factor

$$N = \int_0^\infty \mathrm{d}r\ (g_\kappa^\alpha(r)^2 + f_\kappa^\alpha(r)^2 + g_{-\kappa-1}^\alpha(r)^2 + f_{-\kappa-1}^\alpha(r)^2) \tag{2.19}$$

where sgn means the sign of the integral. The effect of spin polarization mixes states of different j or κ. In a numerical solution of the system of ordinary differential equations (ODE) one has to impose a certain κ character on the boundary condition at the origin. The system evolves according to the relative strength of spin polarization and spin–orbit coupling. The resulting admixture of j' or κ' type determines the two different solutions. ζ_α measures just this admixture in terms of the ratio of the norm of a given α partial state to the norm of the total wave functions. The parameter η_α is a simple measure for the relative signs of the partial states forming a given solution. It is 1 for a bonding state and -1 for an antibonding state.

Next let us turn to the computational method for solving the system of coupled equations for atoms and ions. Two different algorithms have so far been suggested by Cortona *et al* [19] and Ebert [20]. The principle is to avoid a divergence of the asymptotic wave function at large distances during an intermediate iterative cycle. The conventional method therefore is to integrate the radial equations outward and inward and to match the solutions at the classical turning point. The correct energy is determined by this matching. Ebert [20] utilized the matching condition in an application of the Newton–Raphson method. In his algorithm, two outward solutions and two inward solutions are relaxed to fit the matching conditions through iterative cycles.

We suggest a new algorithm to adapt Liberman's program of self-consistent relativistic atomic calculations [29] directly for the spin-polarized relativistic program. Here one inward integration is used. At large distances from the origin the four radial functions are characterized by an exponential form such as [19, 20]

$$\begin{aligned} g_\kappa(r) &= p_\kappa \exp[-\gamma r] & cf_\kappa(r) &= p_\kappa \beta \exp[-\gamma r] \\ g_{-\kappa-1}(r) &= p_{-\kappa-1} \exp[-\gamma r] & cf_{-\kappa-1}(r) &= p_{-\kappa-1}\beta \exp[-\gamma r] \end{aligned} \tag{2.20}$$

with two common factors

$$\gamma = \sqrt{-E^\alpha - (E^\alpha/c)^2} \qquad \text{and} \qquad \beta = -(1 + E^\alpha/c^2)/\gamma.$$

At infinity ($B(\infty) = 0$) the two partial radial functions corresponding to states with κ and $-\kappa - 1$ are controlled independently by the parameters p_κ and $p_{-\kappa-1}$. They give the starting values for the inward integration. For the outward integration we prepare two solutions corresponding to two different combinations in a series expansion [13, 15, 20], which are orthogonalized in the leading term. Each of them includes an independent constant and in our classification a constant q_1 gives a higher-weighting κ partial function while q_2 supplies the dominant $-\kappa - 1$ partial function. From the above-mentioned starting values for inward and outward integration the coupled equations can

be solved straightforwardly using a generalization indicated by Loucks [30]. In detail the radial function at the first six grid points is determined from the starting value using the Runge–Kutta method. Further integration up to the classical turning point is then performed by means of a predictor–corrector scheme such as the Milne method. In the following we denote the outward solution obtained from q_1 and q_2 respectively by $(g_\kappa^{out:1}(r), f_\kappa^{out:1}(r), g_{-\kappa-1}^{out:1}(r), f_{-\kappa-1}^{out:1}(r))$ and $(g_\kappa^{out:2}(r), f_\kappa^{out:2}(r), g_{-\kappa-1}^{out:2}(r), f_{-\kappa-1}^{out:2}(r))$. For the inward solution we use $(g_\kappa^{in}(r), f_\kappa^{in}(r), g_{-\kappa-1}^{in}(r), f_{-\kappa-1}^{in}(r))$.

Next a linear combination of the two partial outward solutions is formed and matched with the inward part:

$$\begin{bmatrix} g_\kappa^{out:1}(r_m) + Ag_\kappa^{out:2}(r_m) \\ f_\kappa^{out:1}(r_m) + Af_\kappa^{out:2}(r_m) \\ g_{-\kappa-1}^{out:1}(r_m) + Ag_{-\kappa-1}^{out:2}(r_m) \\ f_{-\kappa-1}^{out:1}(r_m) + Af_{-\kappa-1}^{out:2}(r_m) \end{bmatrix} \overset{match}{\Longleftrightarrow} \begin{bmatrix} Bg_\kappa^{in}(r_m) \\ Bf_\kappa^{in}(r_m) \\ Cg_{-\kappa-1}^{in}(r_m) \\ Cf_{-\kappa-1}^{in}(r_m) \end{bmatrix}. \tag{2.21}$$

These four matching conditions can be achieved by an adjustment of the three coefficients (A, B, C) and the energy E^α. An effective trial value of A, B and C can be formulated analytically: using the connection between the inward and outward solution in the last two equations of equation (2.21) we obtain the following A and C:

$$A = \frac{g_{-\kappa-1}^{out:1}(r_m) f_{-\kappa-1}^{in}(r_m) - g_{-\kappa-1}^{in}(r_m) f_{-\kappa-1}^{out:1}(r_m)}{g_{-\kappa-1}^{in}(r_m) f_{-\kappa-1}^{out:2}(r_m) - g_{-\kappa-1}^{out:2}(r_m) f_{-\kappa-1}^{in}(r_m)} \tag{2.22}$$

$$C = \frac{g_{-\kappa-1}^{out:1}(r_m) f_{-\kappa-1}^{out:2}(r_m) - g_{-\kappa-1}^{out:2}(r_m) f_{-\kappa-1}^{out:1}(r_m)}{g_{-\kappa-1}^{in}(r_m) f_{-\kappa-1}^{out:2}(r_m) - g_{-\kappa-1}^{out:2}(r_m) f_{-\kappa-1}^{in}(r_m)}. \tag{2.23}$$

From the first line of equation (2.21) an expression for B is given by means of the above-estimated A:

$$B = \frac{g_\kappa^{out:1}(r_m) + Ag_\kappa^{out:2}(r_m)}{g_\kappa^{in}(r_m)}. \tag{2.24}$$

Finally the difference between the inward and outward solution in the second line of equation (2.21) is used for the energy correction. The expression for the relativistic energy correction as outlined by [31, 32] can easily be generalized to the spin-polarized case. The improved trial correction for E_α is then derived as

$$\Delta E = \frac{cBg_\kappa^{in}(r_m)(f_\kappa^{out:1}(r_m) + Af_\kappa^{out:2}(r_m) - Bf_\kappa^{in}(r_m))}{N} \tag{2.25}$$

where N is the normalization factor defined in equation (2.19).

Within the iterative cycle for the energy eigenvalue, the trial coefficients p_κ, $p_{-\kappa-1}$, q_1 and q_2 for the next iteration are then given by the following replacements:

$$\frac{Bp_\kappa}{\sqrt{N}} \longrightarrow p_\kappa \qquad \frac{Bp_{-\kappa-1}}{\sqrt{N}} \longrightarrow p_{-\kappa-1} \qquad \frac{q_1}{\sqrt{N}} \longrightarrow q_1 \qquad \frac{Aq_2}{\sqrt{N}} \longrightarrow q_2. \tag{2.26}$$

The new trial energy E^α is

$$E^\alpha + \Delta E \longrightarrow E^\alpha. \tag{2.27}$$

The procedure for calculating the two different solutions for given values of ℓ and μ is similar to the scheme determining the correct number of nodes in Liberman's programme. Seeking bonding and antibonding states, the trial energies are shifted downward and upward respectively until the corresponding values of η_α are achieved.

When the correct η_α is attained the energy is further refined according to equation (2.27). The convergence criterion for the wave functions and their energies is that A, B and C become unity while ΔE becomes smaller than some tolerance ($<10^{-6}$).

Once the eigenvalue and wave functions for a given potential are determined, the charge densities $n(r)$ and the magnetization densities $m_s(r)$ are constructed as

$$n(r) = \sum_{n\ell\mu\alpha} W^\alpha_{n\ell\mu}(g^{n\mu;\alpha}_\ell(r)^2 + f^{n\mu;\alpha}_\ell(r)^2 + g^{n\mu;\alpha}_{-\ell-1}(r)^2 + f^{n\mu;\alpha}_{-\ell-1}(r)^2) \tag{2.28}$$

and

$$m_s(r) = \sum_{n\ell\mu\alpha} W^\alpha_{n\ell\mu}(g^{n\mu;\alpha}_\ell(r)^2\sigma^\mu_{\ell,\ell} - f^{\mu;\alpha}_\ell(r)^2\sigma^\mu_{-\ell,-\ell} + g^{n\mu;\alpha}_{-\ell-1}(r)^2\sigma^\mu_{-\ell-1,-\ell-1} - f^{n\mu;\alpha}_{-\ell-1}(r)^2\sigma^\mu_{\ell+1,\ell+1} + 2g^{n\mu;\alpha}_\ell(r)g^{n\mu;\alpha}_{-\ell-1}(r)\sigma^\mu_{\ell,-\ell-1}). \tag{2.29}$$

Each of the expressions above is derived by projecting $n(\boldsymbol{r})$, equation (2.2), and the z-component of $\boldsymbol{m}_s(\boldsymbol{r})$, equation (2.5), onto the radial part. Here $W^\alpha_{n\ell\mu}$ (=1 or 0) denotes a weight factor for the $\{n\ell\mu\alpha\}$ state which is determined from the constraint that the sum of one-electron energies be minimized for the given number of electrons:

$$\sum_{n\ell\mu\alpha} W^\alpha_{n\ell\mu}E^\alpha_{n\ell\mu} = \min \tag{2.30}$$

and

$$\sum_{n\ell\mu\alpha} W^\alpha_{n\ell\mu} = Z - N_{ion} \tag{2.31}$$

where N_{ion} is the ionic charge.

As for the self-consistent determination of the effective potential, we adopt Liberman's algorithm [29]. The starting values for the energy of a given $\{n\ell\mu\alpha\}$ state as well as the starting charge and magnetization densities are obtained from a self-consistent solution of the SPDD equation. The relativistic corrections to the exchange–correlation [9, 10] potential are proportional to c^{-2} and r_s^{-3} where r_s is defined in terms of the density as $4\pi r_s^3 a_0^3/3 = 1/n$ and a_0 is the Bohr radius. In practical calculations the relativistic corrections to the exchange–correlation potential are negligibly small; thus for our purposes the von Barth and Hedin expression for the exchange–correlation potential was used [1].

3. Lanthanide and actinide ions

3.1. The energy level and the radial wave function

The solutions of equation (2.2) are a set of non-degenerate orbitals $(nl\mu)$ that are split in a Zeeman-like manner. The initial degeneracy with respect to the z-component of the total angular momentum μ is lifted by the introduction of spin polarization that results in an internal magnetic field. In tables 1 and 2 the calculated results for the energies η_α and ζ_α are collected for lanthanide and actinide ions respectively. As we would like to concentrate on trends in the energy splitting for each series, we have chosen three representative ions: these are $^{58}Ce^{3+}$, $^{60}Nd^{3+}$ and $^{62}Sm^{3+}$ for the lanthanides and $^{90}Th^{3+}$, $^{92}U^{3+}$ and $^{94}Pu^{3+}$ for the actinides. Generally the energies are divided into two groups according to their respective magnitudes. These groups can be characterized by their corresponding bonding parameter η_α as each of them is made up of a distinct combination of partial wave functions of κ and $-\kappa-1$ type. Clearly the states defined to be bonding are lower in energy. For

Table 1. 4f-level energies, η_α and ζ_α, for $^{58}Ce^{3+}$, $^{60}Nd^{3+}$ and $^{62}Sm^{3+}$ in the self-consistent SPCD calculation.

	$^{58}Ce^{3+}$			$^{60}Nd^{3+}$			$^{62}Sm^{3+}$		
μ	Energy	η_α	ζ_α	Energy	η_α	ζ_α	Energy	η_α	ζ_α
5/2	−1.1231	1	0.938	−1.2224	1	0.902	−1.2873	1	0.893
3/2	−1.1203	1	0.868	−1.2202	1	0.796	−1.2908	1	0.778
1/2	−1.1204	1	0.789	−1.2181	1	0.678	−1.2941	1	0.653
−1/2	−1.1189	1	0.693	−1.2157	1	0.546	−1.2972	1	0.516
−3/2	−1.1170	1	0.571	−1.2131	1	0.395	−1.3002	1	0.365
−5/2	−1.1148	1	0.391	−1.2104	1	0.217	−1.3031	1	0.194
−7/2	−1.1117	0	0.000	−1.2073	0	0.000	−1.2836	0	0.000
−5/2	−1.0987	−1	0.609	−1.1494	−1	0.783	−1.1768	−1	0.806
−3/2	−1.0965	−1	0.429	−1.1467	−1	0.605	−1.1734	−1	0.635
−1/2	−1.0947	−1	0.307	−1.1442	−1	0.454	−1.1702	−1	0.486
1/2	−1.0931	−1	0.211	−1.1418	−1	0.322	−1.1671	−1	0.347
3/2	−1.0917	−1	0.132	−1.1396	−1	0.204	−1.1642	−1	0.222
5/2	−1.0904	−1	0.062	−1.1375	−1	0.098	−1.1616	−1	0.107
7/2	−1.0892	0	0.000	−1.1355	0	0.000	−1.1589	0	0.000

Table 2. 5f-level energies, η_α and ζ_α, for $^{90}Th^{3+}$, $^{92}U^{3+}$ and $^{94}Pu^{3+}$ in the self-consistent SPCD calculation.

	$^{90}Th^{3+}$			$^{92}U^{3+}$			$^{94}Pu^{3+}$		
μ	Energy	η_α	ζ_α	Energy	η_α	ζ_α	Energy	η_α	ζ_α
5/2	−1.7932	1	0.977	−2.0425	1	0.945	−2.2665	1	0.932
3/2	−1.7903	1	0.953	−2.0362	1	0.884	−2.2576	1	0.855
1/2	−1.7869	1	0.930	−2.0296	1	0.813	−2.2478	1	0.768
−1/2	−1.7833	1	0.906	−2.0219	1	0.729	−2.2372	1	0.663
−3/2	−1.7791	1	0.885	−2.0130	1	0.621	−2.2250	1	0.531
−5/2	−1.7738	1	0.878	−2.0018	1	0.457	−2.2105	1	0.344
−7/2	−1.7499	0	0.000	−1.9844	0	0.000	−2.1915	0	0.000
−5/2	−1.7418	−1	0.122	−1.9336	−1	0.543	−2.0851	−1	0.656
−3/2	−1.7365	−1	0.115	−1.9226	−1	0.379	−2.0709	−1	0.469
−1/2	−1.7324	−1	0.094	−1.9138	−1	0.271	−2.0590	−1	0.337
1/2	−1.7288	−1	0.070	−1.9062	−1	0.187	−2.0485	−1	0.232
3/2	−1.7256	−1	0.047	−1.8995	−1	0.116	−2.0390	−1	0.145
5/2	−1.7230	−1	0.023	−1.8935	−1	0.055	−2.0303	−1	0.068
7/2	−1.7203	0	0.000	−1.8879	0	0.000	−2.0222	0	0.000

$\mu = \pm 7/2$ the equations are uncoupled because $\sigma^{\mu}_{\kappa,\kappa'} = 0$. In this case, $\eta_\alpha = 0$ denotes the uncoupled state.

Another interesting feature is the ratio of mixing of the two different types of κ or j. This ratio is represented by the parameter ζ_α. It measures the ratio of the $(j = 5/2)$-like partial state and the total radial wave functions. We may take the uncoupled case as an example; when the matrix element $\sigma^{\mu}_{\kappa,\kappa'}$ disappears (as is the case for $\mu = \pm 7/2, \kappa = 3$) the resulting radial wave function will be composed of the $j = 7/2$ partial state only. Since there is no coupling to the $j = 5/2$ state we have $\zeta_\alpha = 0$. Tables 1 and 2 show that the sum of ζ_α for equal μs is unity, except for the case of $\mu = \pm 7/2$ where there is no

$j = 5/2$ contribution. The ratio between the partial states is determined automatically in the self-consistent process. In the upper part of tables 1 and 2 we notice that for a given ion the mixing factor decreases from $\mu = 5/2$ to $\mu = -5/2$. This corresponds to stronger coupling and therefore enhanced admixture of $j = 7/2$ to the solution. While this feature can be accounted for at least qualitatively by the simple dependence on μ of $\sigma^{\mu}_{\kappa,\kappa'}$, the coupling strength mainly depends on the spin polarization of the f shell. Therefore the change of ζ_α for a given ion will be most pronounced for Gd^{3+} and Pu^{3+} where we encounter a half-filled shell and thus a maximum spin moment.

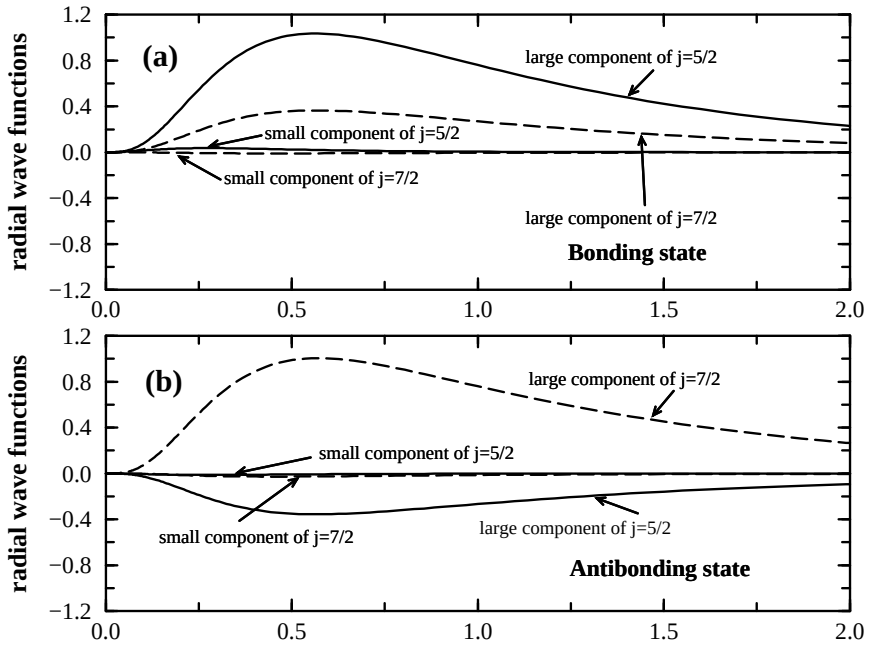

Figure 1. 4f radial wave functions of the $\mu = 5/2$ state in $^{64}Gd^{3+}$ according to the self-consistent SPCD equation. The bonding and antibonding states, each of which corresponds to a different combination between $j = 5/2$ and $7/2$ partial states, are given in (a) and (b) respectively. The solid lines denote the partial wave function of the $j = 5/2$ state and the broken lines denote that of the $j = 7/2$ state.

In figure 1 the 4f radial wave function of Gd^{3+} is shown for $\mu = 5/2$. The bonding state is plotted in (a) while (b) represents the antibonding solution. Solid lines denote the $j = 5/2$ partial radial wave functions, while the broken lines denote the $j = 7/2$ functions. Clearly in the bonding state the two large components $g_\kappa(r)$ and $g_{-\kappa-1}(r)$ of equation (2.2) have the same sign while the antibonding solutions are formed by components of opposite sign. The relative size of the amplitudes of the partial waves correspond to the value of ζ_α in table 2. In figure 2 the 4f and 5f energy levels of the lanthanide and actinide series calculated using the SPCD equation are depicted. As a common feature to both series, the first and last elements show two energy levels with degeneracy six and eight. Since the f shell in these cases is either filled or empty there is no internal field due to spin splitting and thus it is the spin–orbit interaction that causes the splitting.

Moving away from these elements toward the middle of the series corresponds to filling or emptying the f shell and thus creating an internal field. As a consequence the levels are split. While the spectrum to the left is characterized by a splitting into two groups

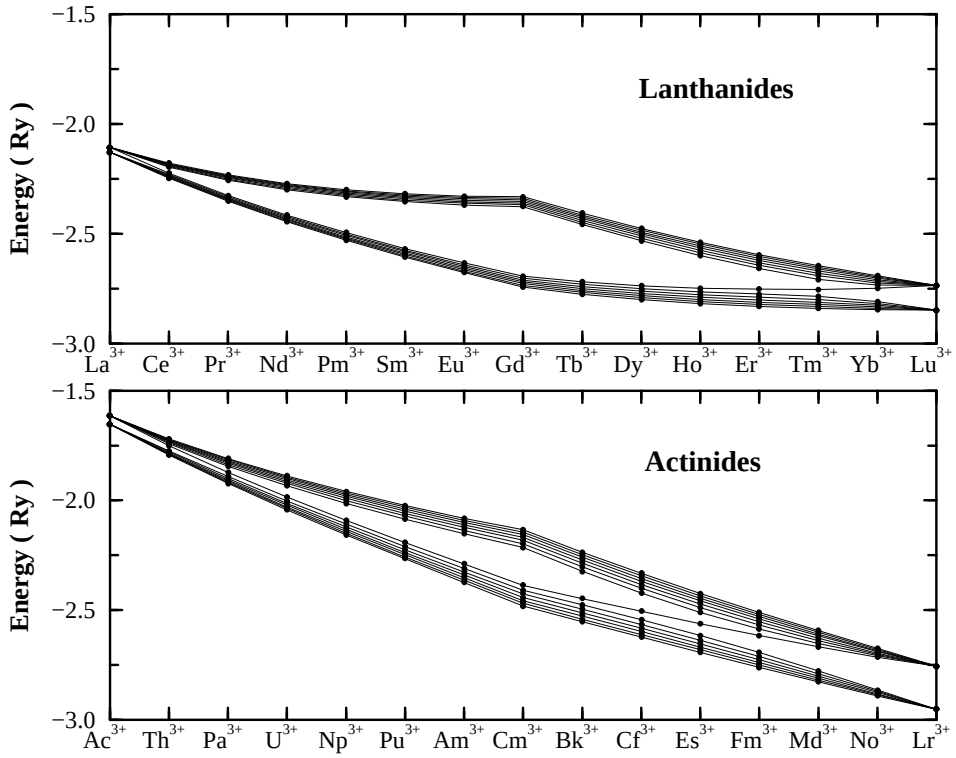

Figure 2. f-level energies for the trivalent ions of the lanthanides and actinides obtained from the self-consistent SPCD calculation.

composed of seven states there is a transition from a 'seven and seven' to a 'six and eight' configuration for the heavier elements. This trend is more pronounced in the group of the actinides than in the lanthanides. The reason for this can be seen in the relative strength of the spin splitting and spin–orbit coupling. For the lanthanides the effect of spin–orbit coupling on the splitting scheme is less pronounced. Only for the late ions from Er^{3+} to Yb^{3+} is there a clear tendency towards what we call the 'relativistic regime'. Most of the ionic levels are governed by the 'exchange regime'. In the actinides the transition in between these two regimes sets in earlier. The enhanced influence of spin–orbit coupling can already be seen from Bk^{3+} on.

In order to clarify the dependence of the level structure on the effects of spin and spin–orbit splitting we calculated the energies of the 5f and 6p shell for the uranium atom using five different approximations, namely the normal Dirac equation without a magnetic field (Dirac), the SPDD (decoupled), the SPCD equation (coupled), the spin-polarized scalar relativistic equation (SP-scalar), and the scalar relativistic equation without a magnetic field (scalar). The exchange–correlation potential used was the same in all cases. The scalar relativistic method has been suggested by several authors [33–36] utilizing different averaging processes for the relativistic states $j = \ell \pm 1/2$. Here we use an expression for the scalar relativistic method derived by Koelling and Harmon [34].

The calculated results for the 5f- and 6p-level energies are shown in figures 3(a) and 3(b) respectively. The sequence of the energies corresponds to the μ-states as shown in table 2. In the Dirac case there are two degenerate levels, whose difference in energy

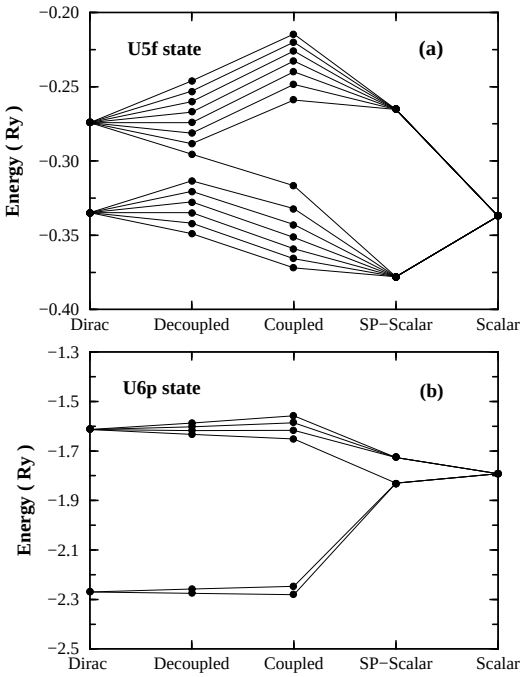

Figure 3. 5f- and 6p-level energies of the U atom in various approximations. The label 'Dirac' represents the normal Dirac equation without the magnetic field, 'Decoupled' represents the SPDD equation, 'Coupled' the SPCD equation, 'SP-Scalar' the spin-polarized scalar relativistic equation, and 'Scalar' the scalar relativistic equation without a magnetic field. The calculated results for the 5f state are shown in (a) and those for the 6p states in (b).

corresponds to the strength of the spin–orbit interaction, denoted by Δ_{rel}. On the right-hand side of figure 3 we have the results obtained using the scalar equation. Since there is no spin–orbit splitting in the scalar relativistic approximation, this state is fully degenerate. The inclusion of spin polarization leads to two levels just like in the Dirac case on the left. Nevertheless the SP-scalar levels are of a different nature as they are produced by the exchange interaction, referred to as Δ_{ex}. As compared with the SP-scalar case the difference in energy between the levels $\mu = \pm 7/2$ in the coupled case can be interpreted as the magnitude of Δ_{ex}. In the decoupled case the two Dirac levels are split due to spin polarization. The resulting energy levels are equidistant, very much like in an independent normal Zeeman splitting of the two initially degenerate $j = 5/2$ and $7/2$ states. Turning to the solutions of the coupled equations we encounter the two groups already mentioned, but the anisotropy splitting depends on μ as would be expected for the anomalous Zeeman effect.

Comparing the energy splitting calculated for the U 5f states with that of the 6p states we note an interesting structural difference. While the results of the coupled equation clearly split the 5f levels into two groups each containing seven states the 6p states are split into groups of four and two. This type of splitting is characteristic for cases where spin–orbit splitting is much stronger than spin polarization. The SPCD equations yields both of these coupling types, i.e. the *relativistic regime* where Δ_{rel} is dominant as well as the *exchange regime* where $\Delta_{rel} \ll \Delta_{ex}$. The influence of these competing effects on the f-level splitting in the lanthanide and actinide series can be seen in figure 2. The relative magnitudes of Δ_{rel}

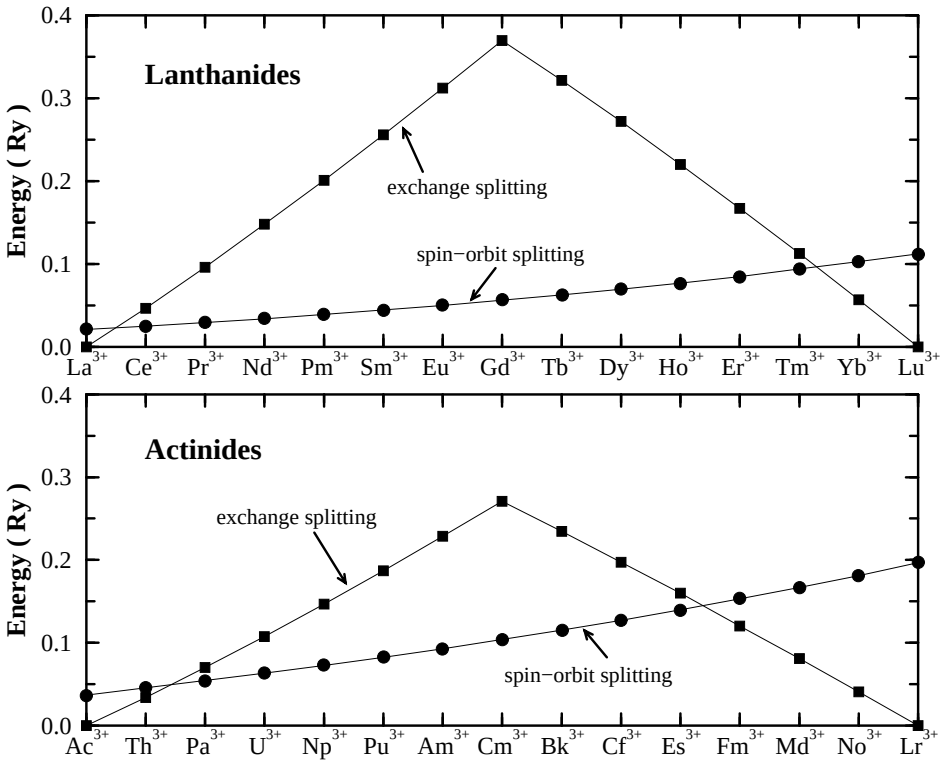

Figure 4. The spin–orbit and exchange splitting parameters of the f state in the trivalent ions of the lanthanides and actinides. The circles and squares represent the calculated values of the spin–orbit and exchange splitting respectively.

and Δ_{ex} for f and p shells are compared in figure 4 and figure 5 respectively. The magnitude of Δ_{ex} in the lanthanide 4f shell is larger than that of the actinide 5f shell. The reason for this can be seen in a stronger degree of localization of the 4f wave function compared with the 5f function. Obviously spin–orbit splitting increases with atomic number, its magnitude for a given ion depending on the potential. Spin polarization on the other hand is due to the filling of the f shell.

As can be seen in figure 5 the p shells in both the lanthanide and the actinide series are clearly situated in the relativistic regime. For the f shells the situation is somewhat more complicated; depending on the occupation number we encounter all three possibilities, the exchange regime, an intermediate-coupling regime as well as the relativistic regime. The discussion of the 4f and 5f energy splitting scheme (figure 2) above already reflected these trends.

Dealing with localized f-electron systems, the question of the degree of localization, as produced by a given calculational scheme, naturally arises. It is well known that simple LSDA alone does not yield a sufficiently precise description of localized systems, as by construction its exchange energy contains self-interaction contributions which gain substantial influence [41, 42] in strongly localized 4f systems. While this work mainly concentrates on the description of the structure and formation of ground-state properties like energy level splittings and wave functions, we would like to add some data allowing for a comparison of the relative position of the energy levels with respect to experiment

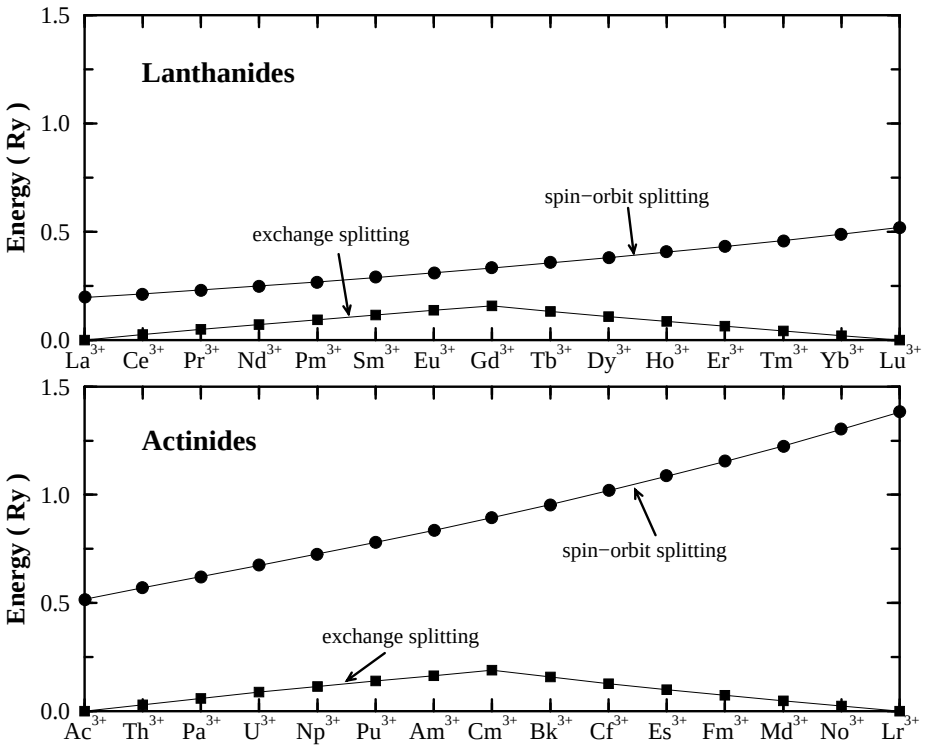

Figure 5. The spin–orbit and exchange splitting parameters of the outer p state in the trivalent ions of the lanthanides and actinides. The circles and squares represent the calculated values of the spin–orbit and exchange splitting respectively.

and other theoretical work. For this purpose we show in tables 5–7 our results for the negative value of the highest occupied molecular orbitals (HOMO) for the atoms and ions of the first half of the lanthanide series. The theoretical data taken from Forstreuter *et al* was [42] produced using a Slater-type orbital expansion to solve for the eigenstates of the spin-polarized Dirac Hamiltonian. In addition to these calculations (RLSDA in tables 5–7) the authors of [42] employed an orbital-dependent potential in order to account for the self-interaction correction (SIC). The experimental data were taken from reference [43]. Generally our results compare well with the RLSDA data. With the exception of that for Pr the HOMOs lie around the RLSDA values or slightly lower. In addition to the eigenvalues, the *l*-character of the highest-lying occupied states is given in brackets with the eigenvalues in tables 5–7. In most cases the RLSDA + SIC calculations lower the eigenvalues by a considerable amount, hence indicating stronger localized orbitals. For a detailed discussion of the effects of employing the SIC, the reader is referred to reference [42].

3.2. Magnetic properties

Let us consider the magnetic properties of the lanthanides and actinides using the SPCD equation of equation (2.2). The ground states of the lanthanides are given by Hund's rules which are described in terms of the Russell–Saunders coupling [12, 37]. The representation of the ground state is given by the total orbital momentum L and spin momentum S. In

Table 3. The ground state of the lanthanide trivalent ions in the SPCD and SPDD equation. $4f^n$ means the occupation number of the 4f shell. The symbol $^{(2S+1)}L_J$ is specified by the lowest multiplet of the Hund's rule. The values of g in the parentheses show an estimate from $^{(2S+1)}L_J$.

			SPCD equation				SPDD equation			
	$4f^n$	$^{(2S+1)}L_J$	L	S	J	g	L	S	J	g
$^{57}La^{3+}$	0	$^1S_0$	0.00	0.00	0.0	0.00 (0.00)	0.00	0.00	0.0	0.0
$^{58}Ce^{3+}$	1	$^2F_{5/2}$	2.98	0.48	2.5	0.86 (0.86)	2.86	0.36	2.5	0.9
$^{59}Pr^{3+}$	2	$^3H_4$	4.97	0.97	4.0	0.81 (0.80)	4.57	0.57	4.0	0.9
$^{60}Nd^{3+}$	3	$^4I_{9/2}$	5.97	1.47	4.5	0.73 (0.73)	5.14	0.64	4.5	0.9
$^{61}Pm^{3+}$	4	$^5I_4$	5.97	1.97	4.0	0.61 (0.60)	4.57	0.57	4.0	0.9
$^{62}Sm^{3+}$	5	$^6H_{5/2}$	4.97	2.47	2.5	0.29 (0.29)	2.86	0.36	2.5	0.9
$^{63}Eu^{3+}$	6	$^7F_0$	2.97	2.97	0.0	0.00 (0.00)	0.00	0.00	0.0	0.0
$^{64}Gd^{3+}$	7	$^8S_{7/2}$	0.03	3.47	3.5	2.00 (2.00)	3.00	0.50	3.5	1.1
$^{65}Tb^{3+}$	8	$^7F_6$	3.04	2.96	6.0	1.50 (1.50)	5.14	0.86	6.0	1.1
$^{66}Dy^{3+}$	9	$^6H_{15/2}$	5.04	2.45	7.5	1.33 (1.33)	6.42	1.07	7.5	1.1
$^{67}Ho^{3+}$	10	$^5I_8$	6.05	1.94	8.0	1.24 (1.25)	6.85	1.14	8.0	1.1
$^{68}Er^{3+}$	11	$^4I_{15/2}$	6.05	1.45	7.5	1.19 (1.20)	6.42	1.07	7.5	1.1
$^{69}Tm^{3+}$	12	$^3H_6$	5.02	0.97	6.0	1.16 (1.17)	5.14	0.86	6.0	1.1
$^{70}Yb^{3+}$	13	$^2F_{7/2}$	3.00	0.50	3.5	1.14 (1.14)	3.00	0.50	3.5	1.1
$^{71}Lu^{3+}$	14	$^1S_0$	0.00	0.00	0.0	0.00 (0.00)	0.00	0.00	0.0	0.0

Table 4. The ground state of the actinide trivalent ions in the SPCD equation. $5f^n$ represents the occupation number of the 5f shell. The symbol $^{(2S+1)}L_J$ is specified by the lowest multiplet of the Hund's rule. The values of g in the parentheses denote an estimate from $^{(2S+1)}L_J$.

	$5f^n$	$^{(2S+1)}L_J$	L	S	J	g
$^{90}Th^{3+}$	1	$^2F_{5/2}$	2.95	0.45	2.5	0.87 (0.86)
$^{91}Pa^{3+}$	2	$^3H_4$	4.90	0.90	4.0	0.82 (0.80)
$^{92}U^{3+}$	3	$^4I_{9/2}$	5.86	1.36	4.5	0.75 (0.73)
$^{93}Np^{3+}$	4	$^5I_4$	5.82	1.82	4.0	0.64 (0.60)
$^{94}Pu^{3+}$	5	$^6H_{5/2}$	4.79	2.29	2.5	0.34 (0.29)
$^{95}Am^{3+}$	6	$^7F_0$	2.78	2.78	0.0	0.00 (0.00)
$^{96}Cm^{3+}$	7	$^8S_{7/2}$	0.19	3.31	3.5	1.94 (2.00)
$^{97}Bk^{3+}$	8	$^7F_6$	3.25	2.75	6.0	1.46 (2.00)
$^{98}Cf^{3+}$	9	$^6H_{15/2}$	5.27	2.23	7.5	1.30 (1.33)
$^{99}Es^{3+}$	10	$^5I_8$	6.23	1.76	8.0	1.21 (1.25)
$^{100}Fm^{3+}$	11	$^4I_{15/2}$	6.16	1.34	7.5	1.17 (1.20)
$^{101}Md^{3+}$	12	$^3H_6$	5.07	0.93	6.0	1.15 (1.17)
$^{102}No^{3+}$	13	$^2F_{7/2}$	3.00	0.50	3.5	1.14 (1.14)
$^{103}Lw^{3+}$	14	$^1S_0$	0.00	0.00	0.0	0.00 (0.00)

the SPCD scheme, L and S respectively are defined as

$$L = \left| \int \mathrm{d}\boldsymbol{r}\ \langle \Psi | \hat{\psi}^\dagger(\boldsymbol{r}) \beta \hat{\boldsymbol{\ell}} \hat{\psi}(\boldsymbol{r}) | \Psi \rangle \right| = \left| \int_0^\infty \mathrm{d}r\ m_\ell(r) \right| \tag{3.1}$$

and

$$S = \frac{1}{2} \left| \int_0^\infty \mathrm{d}r\ m_s(r) \right| \tag{3.2}$$

Table 5. Comparison of theoretical values of the negative HOMO and experiment values for the ionization potentials IP_1 of free atoms in eV. 'RLSDA' indicates spin-polarized relativistic density functional calculations employing a Slater-type orbital expansion.

	^{58}Ce	^{59}Pr	^{60}Nd	^{61}Pm	^{62}Sm	^{63}Eu	^{64}Gd
HOMO SPCD (present)	4.4 (d)	3.0 (f)	3.7 (f)	4.2 (f)	4.6 (s)	4.7 (s)	4.2 (d)
HOMO RLSDA [42]	3.8	3.8	3.8	3.8	3.8	3.9	4.2
HOMO RLSDA SIC [42]	5.3	5.0	5.1	5.1	5.2	5.2	5.7
(Experiment) [43]	5.5	5.4	5.5	5.6	5.6	5.7	6.1

Table 6. Comparison of theoretical values of the negative HOMO and experiment values for the ionization potentials IP_1 of free R^+ ions in eV.

	^{58}Ce	^{59}Pr	^{60}Nd	^{61}Pm	^{62}Sm	^{63}Eu	^{64}Gd
HOMO SPCD (present)	9.4 (d)	8.9 (f)	9.7 (f)	10.3 (f)	10.9 (f)	11.1 (s)	10.6 (d)
HOMO RLSDA [42]	8.2	9.1	9.2	9.3	9.5	9.6	10.5
HOMO RLSDA SIC [42]	10.8	10.4	10.6	10.7	10.9	11.0	12.1
(Experiment) [43]	10.9	10.6	10.7	10.9	11.1	11.2	12.1

Table 7. Comparison of theoretical values of the negative HOMO and experiment values for the ionization potentials IP_1 of free R^{2+} ions in eV.

	^{58}Ce	^{59}Pr	^{60}Nd	^{61}Pm	^{62}Sm	^{63}Eu	^{64}Gd
HOMO SPCD (present)	15.1 (f)	16.2 (f)	17.0 (f)	17.8 (f)	18.4 (f)	18.9 (f)	17.9 (d)
HOMO RLSDA [42]	14.1	15.2	16.0	16.8	17.4	17.9	16.4
HOMO RLSDA SIC [42]	22.0	23.4	24.7	25.8	26.7	27.7	19.5
(Experiment) [43]	20.2	21.6	22.1	22.3	23.4	24.9	20.6

where $m_s(r)$ indicates the spin-magnetization density as in equation (2.29). $m_\ell(r)$ is defined by the radial wave functions obtained from the self-consistent calculation:

$$m_\ell(r) = \sum_{n\ell\nu\alpha} W^\alpha_{n\ell\mu}(g^{n\mu;\alpha}_\ell(r)^2\ell^\mu_{\ell,\ell} - f^{\mu;\alpha}_\ell(r)^2\ell^\mu_{-\ell,-\ell} + g^{n\mu;\alpha}_{-\ell-1}(r)^2\ell^\mu_{-\ell-1,-\ell-1} - f^{n\mu;\alpha}_{-\ell-1}(r)^2\ell^\mu_{\ell+1,\ell+1} + 2g^{n\mu;\alpha}_\ell(r)g^{n\mu;\alpha}_{-\ell-1}(r)\ell^\mu_{\ell,-\ell-1}). \tag{3.3}$$

Here the matrix $\ell^\mu_{\kappa,\kappa'}$ stands for

$$\langle\chi^\mu_\kappa|\hat{\ell}_z|\chi^{\mu'}_{\kappa'}\rangle = \ell^\mu_{\kappa\kappa'}\delta_{\mu\mu'} = \begin{cases} (\kappa+1)u_{\kappa\mu} & \text{for } \kappa' = \kappa \\ \dfrac{1}{2}\sqrt{1-u^2_{\kappa\mu}} & \text{for } \kappa' = -\kappa-1 \end{cases} \tag{3.4}$$

where $u_{\kappa\mu}$ is defined in equation (2.16). Using the definitions of L, equation (3.1), and S, equation (3.2), we obtain the total angular momentum J as

$$J = \left|\int_0^\infty \mathrm{d}r\,\left(m_\ell(r) + \frac{m_s(r)}{2}\right)\right|. \tag{3.5}$$

In table 3 we give the calculated values of L, S and J for the lanthanide trivalent ions. The lowest-lying J-multiplet is denoted in the usual way as $^{(2S+1)}L_J$. We understand that the values for L, S and J calculated from the SPCD equation are in very good agreement with Hund's rules. Accordingly we can say that the ground state of the SPCD equation

produces the Hund's rule for the lanthanides. The observable magnetic values—for example, the effective Bohr magneton number, $p = g\sqrt{J(J+1)}$ [38]—contain the g-factor and J. This g-factor is what is called the Landé factor. Table 3 also shows the g-values evaluated by the SPCD equation together with those of Hund's rules in parentheses. These values are almost equal and therefore the calculated magnetic values agree quite well with those obtained from Hund's rules. In table 3 another notable point is that the moments calculated using the decoupled scheme SPDD deviate from the values expected on the basis of Hund's rules. The deviation of S and L is complementary in such a way that the value of J is conserved for each ion. Although it is impossible to evaluate the g-value of La^{3+}, Eu^{3+} and Lu^{3+} for $J = 0$, the other g-values estimated from the SPDD equation are nearly constant around 1 and thus we can confirm that the value of S comes out like in a normal Zeeman effect. The reason for this is the poor outcome of the spin moment through the self-consistent process, as in the decoupled calculation we restrict the system to a certain value of j. From the different properties of the SPCD and SPDD equations we see that it is the coupling of $j = \ell \pm 1/2$ states that gives rise to the anomalous Zeeman effect and therefore plays an essential part in the moment formation according to Hund's rules.

Next let us move to the actinide trivalent ions. In table 4 the values of L, S and J calculated from the SPCD equation for the series of actinide ions are shown together with the corresponding g-factors. The ground-state moments L, S and J are characterized according to Hund's rules, although their values seem to deviate slightly compared with the lanthanides of table 3. The same is true for the estimated g-values given in table 3 which are listed in parentheses. However, on the whole we may propose that the magnetic properties of the actinide ions are reasonably well described by Hund's rules.

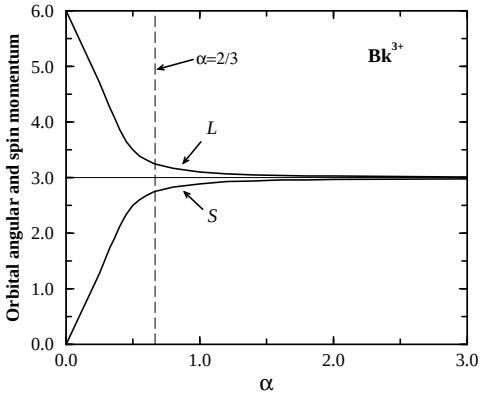

Figure 6. The dependence of the exchange potential on the orbital angular and spin momenta for Bk^{3+}. The parameter α denotes the Slater X_α exchange parameter.

From figure 4 it can be seen that this tendency depends on the relative strength of spin–orbit coupling and spin splitting through the series of 5f ions. In order to reveal the dependence of S and L on the exchange potential we made the following numerical experiment. For Bk^{3+} for which the ground-state spin and orbital moment deviation from Hund's rule is strongest, we performed trial calculations employing Slater's X_α exchange potential [39] with varying magnitude of α. The omission of the correlation part of the potential for the duration of these test calculations has no influence on the moment formation. The results are shown in figure 6. Here Slater's exchange potential for $\alpha = 3/2$ corresponds to the LDA limit. When α increases above the LDA value each of L and S approaches

the value of 3 as is expected from Hund's rules. With decreasing α, S goes to zero while L approaches 6 as the total J is stable and equal to 6. We can therefore conclude that the magnitude of S and L depends entirely on the strength of the exchange potential.

It is well known that the Hamiltonian of equation (2.13) does not commute with S and L but only with the total angular momentum J. However, judging from our calculations, L and S seem to be good quantum numbers, as long as the Russell–Saunders coupling is valid for the case in question. A key role in these systems is played by Δ_{rel} and Δ_{ex}. As mentioned in section 3.1 almost all ions of the lanthanides and actinides belong to the exchange regime, as their internal magnetic field dominates spin–orbit splitting. Thus in a first approximation the spin–orbit interaction can be neglected and consequently the projections of the orbital angular momentum and spin on the z-axis are conserved. Under the influence of a strong magnetic field the level splitting is known to be described by the orbital angular momentum and spin rather than the total angular momentum and the Landé factor [40]. This phenomenon is called the Paschen–Back effect [24]. We therefore argue that the relative size of Δ_{rel} and Δ_{ex} due to the interplay of spin–orbit coupling and the internal magnetic field leads to a situation where the Russell–Saunders coupling holds despite the obvious importance of relativistic effects for these f-electron systems.

4. Summary and discussion

On the basis of the SPRDF the magnetic properties of the lanthanide and actinide trivalent ions have been investigated by means of a detailed description of their energy level scheme and ground-state wave functions using the spin-only Dirac formalism within SPRDF theory. Since the relativistic corrections to the exchange–correlation potential are small they were neglected for our purposes. In the case of spherical boundary conditions, such as apply to atoms and ions, the SPRDF produces the SPCD equations. The mixing of states $j = \ell \pm 1/2$ is a characteristic feature of the SPCD equation and turns out to lie at the heart of the physical trends observed in the 4f and the 5f series. It is indeed the origin of the anomalous Zeeman effect which dominates the energy scheme for lanthanide and actinide ions.

The values of L, S and J obtained from our self-consistent SPCD calculations demonstrate the validity of Hund's rules for all trivalent ions of these series. The magnitude of S is governed by the strength of the exchange potential while L changes as a function of S. J is a conserved quantity. This suggests that the exchange potential of the LDA is capable of yielding S in agreement with Hund's rules for f-electron systems. We have shown that despite the large relativistic effects in 4f and 5f systems their ground-state properties are mainly governed by the exchange interaction. Hence S and L can be regarded as remaining good quantum numbers, and the magnetic properties of these systems are well described using the Russell–Saunders coupling scheme.

In a non-relativistic scheme, Hund's rules are established by means of configuration effects in Hartree–Fock theory [22]. Their origin can be seen in the exchange described by the Fock term involving different orbitals. The non-local potential originating from this term yields an orbital dependence of the energy, and the minimum Hartree–Fock energy can be related to the values of L and S according to Hund's rules. In the SPRDF scheme the origin of the magnetic field is also the electron exchange and correlation, but the anisotropic orbital dependence which is important for Hund's rules stems from relativistic effects. Although both schemes are capable of explaining Hund's rules we would like to stress that the underlying reasons for this are quite different. Since the one-particle equation in the SPRDF—here the SPCD equation—is formulated in a local form, the corresponding electronic configuration can be determined by simply minimizing the sum of the one-electron

levels. The self-consistent calculation then produces a ground state as predicted by Hund's rule.

Finally we would like to comment on an approximate treatment of the SPCD equations for solids. For conduction bands which might under certain circumstances include f bands in the lanthanides and actinides, we know that exchange effects dominate over the effects of spin–orbit coupling. Therefore we can expect a scalar relativistic approach treating spin–orbit interaction at the variational level to provide reliable results. However, since all core electrons belong to the relativistic regime, the Dirac equation rather than the spin-polarized scalar relativistic (SPSR) equation should be employed when solving for energies and wave functions. The failures of the SPSR equation for the 6p state of Pd have already been pointed out by MacDonald, Pickett and Koelling [36]. The importance of the SPCD equation for the description of these states is also strongly suggested by our results.

Acknowledgments

We gratefully acknowledge fruitful discussions with Dr L M Sandratskii. One of us (HY) wishes to thank the Alexander von Humboldt Stiftung for financial support.

References

[1] von Barth U and Hedin L 1972 *J. Phys. C: Solid State Phys.* **5** 1629
[2] Gunnarsson O and Lundqvist B I 1976 *Phys. Rev.* B **13** 4274
[3] Dreizler R M and Gross E K U 1990 *Density Functional Theory* (Berlin: Springer)
[4] Desclaux J P and Freeman A J 1984 *Handbook on the Physics and Chemistry of the Actinides* vol 1, ed A J Freeman and G H Lander (Amsterdam: Elsevier Science)
[5] Rajagopal A K and Callaway J 1973 *Phys. Rev.* B **7** 1912
[6] MacDonald A H and Vosko S H 1979 *J. Phys. C: Solid State Phys.* **12** 2977
[7] Rajagopal A H 1978 *J. Phys. C: Solid State Phys.* **11** L943
[8] Ramana M V and Rajagopal A K 1979 *J. Phys. C: Solid State Phys.* **12** L845
[9] MacDonald A H 1983 *J. Phys. C: Solid State Phys.* **16** 3869
[10] Xu B X, Rajagopal A K and Ramana M V 1984 *J. Phys. C: Solid State Phys.* **17** 1339
[11] Eschrig H, Seifert G and Ziesche P 1985 *Solid State Commun.* **56** 777
[12] Elliot R J 1972 *Magnetic Properties of Rare Earth Metals* (London: Plenum)
[13] Feder R, Rosicky F and Ackermann B 1983 *Z. Phys.* B **52** 31
[14] Ackermann B and Feder R 1984 *Solid State Commun.* **49** 489
[15] Strange P, Staunton J and Gyorffy B L 1984 *J. Phys. C: Solid State Phys.* **17** 3355
[16] Schalder G, Alberts R C, Boring A M and Weinberger P 1987 *Phys. Rev.* B **35** 4324
[17] Jenkins A C and Strange P 1994 *J. Phys.: Condens. Matter* **6** 3499
[18] Solovyev I V, Lichtenstein A I, Gubanov V A, Antropov V P and Andersen O K 1991 *Phys. Rev.* B **43** 14 414
[19] Cortona P, Doniach S and Sommers C 1985 *Phys. Rev.* B **31** 2842
[20] Ebert H 1989 *J. Phys.: Condens. Matter* **1** 9111
[21] See, for example,
Ashcroft N W and Mermin N D 1981 *Solid State Physics* (Tokyo: Holt-Saunders)
[22] Slater J C 1929 *Phys. Rev.* **34** 1293
[23] Slater J C 1963 *Quantum Theory of Molecules and Solids* (New York: McGraw-Hill)
[24] Condon E U and Shortley G H 1970 *The Theory of Atomic Spectra* (Cambridge: Cambridge University Press)
[25] Rose M 1961 *Relativistic Electron Theory* (New York: Addison-Wesley)
[26] Hohenberg P and Kohn W 1964 *Phys. Rev.* B **136** 864
[27] Kohn W and Sham L J 1965 *Phys. Rev.* **140** A1133
[28] Baym G 1969 *Lectures on Quantum Mechanics* (New York: Benjamin) p 552
[29] Liberman D, Waber J T and Cromer D T 1965 *Phys. Rev.* **137** A27
Liberman D, Cromer D T and Waber J T 1971 *Comput. Phys. Commun.* **2** 107
[30] Loucks T L 1967 *Augmented Plane Wave Method* (New York: Benjamin)

[31] Mayers D J 1957 *Proc. R. Soc.* A **241** 93
[32] Cohen S 1960 *Phys. Rev.* **118** 489
[33] Wood J H and Boring A M 1978 *Phys. Rev.* **18** 2701
[34] Koelling D D and Harmon B N 1977 *J. Phys. C: Solid State Phys.* **10** 3107
[35] Takeda T 1978 *Z. Phys.* B **32** 43
[36] MacDonald A H, Pickett W E and Koelling D D 1980 *J. Phys. C: Solid State Phys.* **13** 2675
[37] Jensen J and Mackintosh A R 1991 *Rare Earth Magnetism* (Oxford: Clarendon)
[38] Kubo R and Nagamiya T 1969 *Solid State Physics* (New York: McGraw-Hill) p 451
[39] Slater J C 1974 *The Self-consistent Field for Molecules and Solids* (New York: MacGraw-Hill)
[40] Landau L D and Lifshitz E M 1965 *Quantum Mechanics* (Oxford: Pergamon) §112, p 427
[41] Perdew J P and Zunger A 1981 *Phys. Rev.* B **28** 5992
[42] Density-functional calculations for rare-earth atoms and ions; see
Forstreuter J, Steinbeck L, Richter M and Eschrig H 1997 *Phys. Rev.* B **55** 9415
[43] Martin W C, Hagan L, Reader J and Sugar J 1974 *J. Phys. Chem. Ref. Data* **3** 771